Distinct roles for dynein light intermediate chains in neurogenesis, migration, and terminal somal translocation

João Carlos Gonçalves[1,2,3] [ID], Tiago J. Dantas[1,4,5] [ID], and Richard B. Vallee[1] [ID]

Cytoplasmic dynein participates in multiple aspects of neocortical development. These include neural progenitor proliferation, morphogenesis, and neuronal migration. The cytoplasmic dynein light intermediate chains (LICs) 1 and 2 are cargo-binding subunits, though their relative roles are not well understood. Here, we used in utero electroporation of shRNAs or LIC functional domains to determine the relative contributions of the two LICs in the developing rat brain. We find that LIC1, through BicD2, is required for apical nuclear migration in neural progenitors. In newborn neurons, we observe specific roles for LIC1 in the multipolar to bipolar transition and glial-guided neuronal migration. In contrast, LIC2 contributes to a novel dynein role in the little-studied mode of migration, terminal somal translocation. Together, our results provide novel insight into the LICs' unique functions during brain development and dynein regulation overall.

Introduction

Cytoplasmic dynein 1 (hereafter "dynein") carries out a very extensive range of functions in the cell. Several dynein-dependent mechanisms are required for vertebrate brain development (Bertipaglia et al., 2018), and impaired dynein function has been associated with multiple neurodevelopmental diseases (Reiner et al., 1993; Lipka et al., 2013; Poirier et al., 2013; Fiorillo et al., 2014; Jamuar et al., 2014). Dynein is essential for the proliferation of embryonic neural stem cells, known as radial glial progenitors (RGPs; Tsai et al., 2005, 2010), which give rise to most neurons and glia in the cerebral cortex (Kriegstein and Alvarez-Buylla, 2009). RGPs have a unique morphology, with an apical process contacting the ventricular surface (VS) and a basal process extending to the pial surface. RGP nuclei oscillate in synchrony with cell cycle progression, a behavior termed interkinetic nuclear migration (INM). During INM, the RGP nuclei migrate away from the VS throughout G1 (basal migration) and return to the VS during G2 (apical migration). Apical INM in RGPs is driven by nuclear envelope-associated dynein, and mitotic entry occurs only when the RGP nucleus has reached the VS (Hu et al., 2013; Baffet et al., 2015; Doobin et al., 2016).

Neurons originating from RGP divisions migrate out of the inner neocortical proliferative region, the ventricular zone (VZ), to the subventricular and intermediate zones (SVZ/IZ), where they at first adopt a multipolar morphology. Multipolar cells require dynein for transition into bipolar neurons and for their subsequent glial-guided migration to the cortical plate (CP) along the basal processes of the RGPs (Shu et al., 2004; Tsai et al., 2005, 2007). In the outermost region of the CP, neurons engage in a final form of non–glial-guided migration called terminal somal translocation (Nadarajah et al., 2001; Franco et al., 2011; Sekine et al., 2011). Whether dynein also contributes to this final stage of neuronal migration is unknown.

How a single form of dynein may carry out such a wide range of functions has been a central question in the field. Dynein has several subunits, which contribute to cargo binding and motor regulation. The function of one class of cytoplasmic dynein-specific subunits, the light intermediate chains (LICs), remains poorly understood. In vertebrates, two highly similar genes, *DYNC1LI1* and *DYNC1LI2* (Pfister et al., 2006), encode LIC1 and LIC2, respectively, which integrate into the dynein complex. The divergent LIC3 (*DYNC2LI1*) associates exclusively to ciliary cytoplasmic dynein-2 to mediate intraflagellar transport (Grissom et al., 2002; Mikami et al., 2002; Taylor et al., 2015). Recently, LIC1 and LIC2 have been shown to link dynein to an emerging class of dynein cargo adaptor proteins, which include the BicD and Hook proteins, RILP, and Spindly (Fig. 1, A and B; Scherer et al., 2014; Schroeder et al., 2014; Schroeder and Vale, 2016; Gama et al., 2017; Lee et al., 2018). These adaptors serve specifically to

[1]Department of Pathology and Cell Biology, Columbia University Medical Center, New York, NY; [2]Life and Health Sciences Research Institute (ICVS), School of Medicine, University of Minho, Braga, Portugal; [3]ICVS/3B's - PT Government Associate Laboratory, Braga/Guimarães, Portugal; [4]I3S - Instituto de Investigação e Inovação em Saúde, University of Porto, Porto, Portugal; [5]IBMC - Instituto de Biologia Molecular e Celular, University of Porto, Porto, Portugal.

Correspondence to Richard B. Vallee: rv2025@columbia.edu.

recruit supercomplexes of dynein and its regulators to diverse forms of subcellular cargo (for review, see Reck-Peterson et al., 2018). Some studies have addressed LIC1- versus LIC2-dynein roles in cultured cells and mainly suggested overlapping functions (Palmer et al., 2009; Tan et al., 2011; Raaijmakers et al., 2013; Jones et al., 2014). To determine the relative functions of LIC1 and LIC2 in vivo, we have examined their requirement during neocortical development. We find that LIC1 and LIC2 each play essential but only partially overlapping roles in neurogenesis and neuronal migration, and we identify a novel role for dynein and LIC2 in the little-explored mechanism of terminal somal translocation.

Results and discussion

Effects of LIC1 and LIC2 depletion in RGP apical nuclear migration

To investigate whether the LIC proteins have distinct or overlapping roles in RGP INM, we delivered shRNAs against *Dync1li1* (LIC1) and/or *Dync1li2* (LIC2) into the lateral ventricles of embryonic day 16 (E16) rat embryos, using in utero electroporation. Analysis of the VZ in electroporated brain slices was performed 4 d after electroporation, at E20. RNAi efficiency was determined by quantitative RT-PCR (qRT-PCR) and immunoblotting (Fig. S1, A and B), which confirmed successful reduction in mRNA and protein levels, respectively. LIC1 knockdown (KD) caused a pronounced shift in the distribution of RGP nuclei away from the VS (Fig. 1, C and D), consistent with inhibition of apical INM. We also observed a marked decrease in mitotic index (Fig. 1 F), consistent with the inability of the nuclei to reach the VS and enter mitosis. To test LIC1 function in apical INM more directly, we performed live imaging of LIC1-depleted RGPs in brain slices. LIC1 KD severely inhibited RGP apical nuclear migration, arresting nuclei before they could reach the VS (Fig. 1 G and Videos 1 and 2). Previous work from our laboratory (Hu et al., 2013) revealed that RGP nuclei may arrest far from (>30 µm) or near to (<10 µm) the VS following expression of shRNAs against genes that mediate early G2 versus late G2 nuclear envelope dynein recruitment. We found that LIC1 KD arrested RGP nuclei at similar distances to those found upon depletion of early G2-dynein recruitment proteins (Fig. 1 E), such as BicD2 (Hu et al., 2013), an LIC interactor protein (Schroeder et al., 2014; Lee et al., 2018).

Increasing dynein recruitment to the nuclear envelope by BicD2 overexpression overcomes KD of genes in the late G2-dynein–recruitment pathway (Hu et al., 2013; Doobin et al., 2016). To examine the functional relationship between BicD2 and LIC1 in our system, we tested whether BicD2 expression could rescue the effects of LIC1 KD. BicD2 overexpression in a LIC1 KD background failed to restore normal nuclear distribution (Fig. 1, H and I). This result is consistent with a common role for BicD2 and LIC1 in apical INM.

In contrast to our LIC1 KD results, LIC2 KD had no detectable effect on RGP apical nuclear migration or mitosis (Fig. 1, C–G; and Video 3). To address whether depletion of both subunits would cause more severe effects on RGP nuclear distribution, we coexpressed shRNAs for LIC1 and LIC2. Reduced levels of both subunits phenocopied LIC1 KD alone (Fig. 1, C–F), supporting a predominant role for LIC1 in apical INM. To test whether these results might reflect differences in LIC1 versus LIC2 protein levels, we measured the relative amounts of dynein subunits in brain lysates during late embryogenesis and adulthood (Fig. S1, C and D). The ratio of LIC1 to LIC2 protein levels was unaltered across developmental stages. In addition, staining of E20 brain slices with LIC1- or LIC2-specific antibodies showed cytoplasmic expression throughout the several layers of the developing neocortex for both subunits (Fig. S1, E–H). Therefore, the effects of LIC1 versus LIC2 KD are likely to result from differential LIC physiological roles.

Mechanistic insight from the LIC functional domains

To test the relative cargo-binding role of the LICs more directly, we generated cDNAs encoding individual LIC functional domains, the N-terminal GTPase-like domain (G domain) and the C-terminal Adaptor domain (A domain; Fig. 1 B). The G domain of each LIC coimmunoprecipitated the dynein heavy chain (HC) and the intermediate chain (IC), but not the endogenous LICs (Fig. S2, A and B). This suggests that expression of the G domain competes with the endogenous LICs for a common HC-binding site. The C-terminal A domain binds directly to BicD2 and other dynein adaptor proteins, but does not coimmunoprecipitate the dynein complex (Schroeder et al., 2014; Gama et al., 2017; Lee et al., 2018).

To understand further the functional roles of the LICs, we electroporated the full-length G domain and A domain versions of each LIC. Expression of the LIC1 or LIC2 A domains had no detectable effect in RGP nuclear distribution or mitotic index (Fig. S2, C–E). Interestingly, expression of full-length LIC1 caused a moderate shift in the RGP nuclei toward the VS (Fig. 2, A and B), consistent with enhanced dynein activity in apical nuclear migration. We observed no such effect for LIC2 (Fig. 2, A and B). In contrast, expression of the LIC1 G domain caused a marked displacement of RGP nuclei away from the VS at distances similar to those seen with LIC1 KD (>30 µm). The LIC1 G domain also caused a strong reduction in mitotic index (Fig. 2, A–D). Surprisingly, despite the common LIC binding site within the HC (Tynan et al., 2000b), the LIC2 G domain had no apparent effect on RGP nuclear position or mitotic index (Fig. 2, A–D). Together, these results confirm a more important cargo-binding role for LIC1 in INM, consistent with the LIC1 and LIC2 KD effects.

LIC1 and LIC2 share high sequence similarity within both dynein- and cargo-binding domains (Tynan et al., 2000a; Pfister et al., 2006). Thus, despite the differences in LIC1 versus LIC2 KD effects, we asked whether LIC2 could compensate for LIC1 depletion. To test this possibility, we coexpressed LIC1 shRNA with a control vector or RNAi-insensitive LIC1 or LIC2 cDNA. Electroporation of LIC1 cDNA on a LIC1 KD background-rescued RGP nuclear position and mitotic index (Fig. 2, E–H). Remarkably, expression of LIC2 cDNA on a LIC1 KD background was able to rescue RGP nuclei position and mitotic index to levels observed with the GFP control (Fig. 2, E–H). However, when compared with LIC1 self-rescue, LIC2 rescue of LIC1 KD showed RGP nuclei slightly, but significantly, shifted away from the VS (Fig. 2, E and F). This again suggests that apical INM is preferentially mediated by LIC1, but increased amounts of LIC2 can overcome LIC1 depletion and restore apical INM.
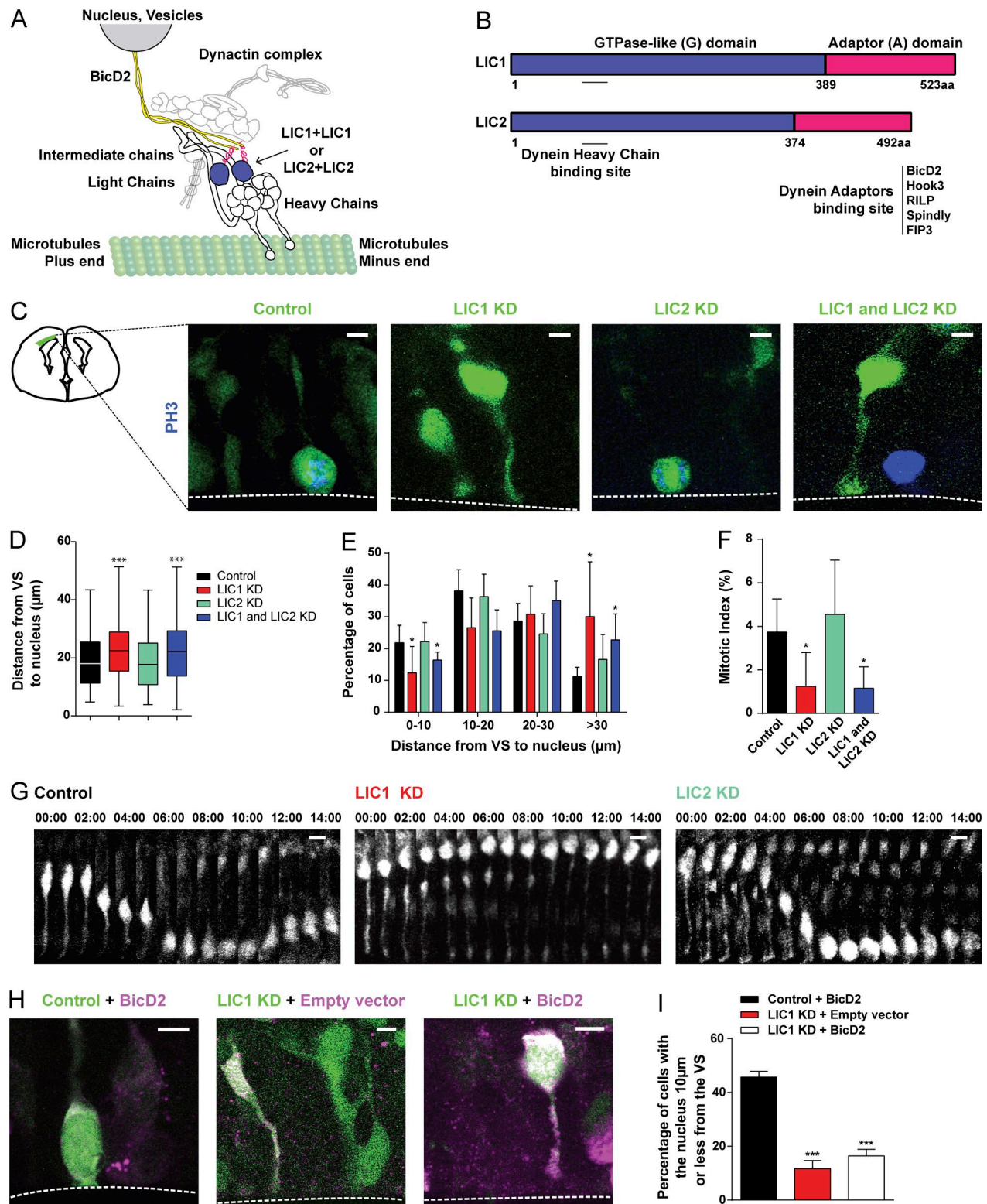
Gonçalves et al.
Dynein LIC1 and LIC2 in neocortical development

Journal of Cell Biology 809
https://doi.org/10.1083/jcb.201806112

Figure 1. **Distinct roles for the LICs in apical INM. (A and B)** Diagrammatic representation of the dynein-dynactin-BicD2 complex (A is modified from Carter et al., 2016). LIC1 versus LIC2 content defines distinct dynein subfractions (Tynan et al., 2000a). **(B)** LIC functional domains and interactors. **(C–G)** E16 rat brains were in utero electroporated with control vector or shRNAs for LIC1 and/or LIC2 and subsequently imaged live or fixed 4 d post injection (d.p.i.), at E20. **(C)** Fixed images of the VZ from electroporated brains stained for the mitotic marker phosphohistone-H3 (PH3). Dashed line represents the VS. **(D, E, and I)** Quantification of distance between the RGP nuclei and the VS across conditions. **(F)** Effect of LIC1 and/or LIC2 KD on RGP cell mitotic index. **(G)** Time-lapse images for control, LIC1 KD, or LIC2 KD in RGPs (Videos 1, 2, and 3). Images are shown with 60-min intervals (hh:mm). **(H and I)** E16 brains were in utero electroporated with BicD2 on a wild-type or LIC1 KD background or LIC1 KD alone. Analysis was done 4 d.p.i. **(H)** Representative images from electroporated RGPs in the VZ. Data presented as box and whiskers plot in D; and data shown as mean ± SD in E, F, and I. Unpaired t test was used in D, E, F and I. (*, P < 0.05; ***, P < 0.001). Data in D, E, and F include at least 337 RGPs from at least five embryos, and data in I include at least 165 RGPs from at least four embryos. Bars: 5 μm (C and H); 10 μm (G).
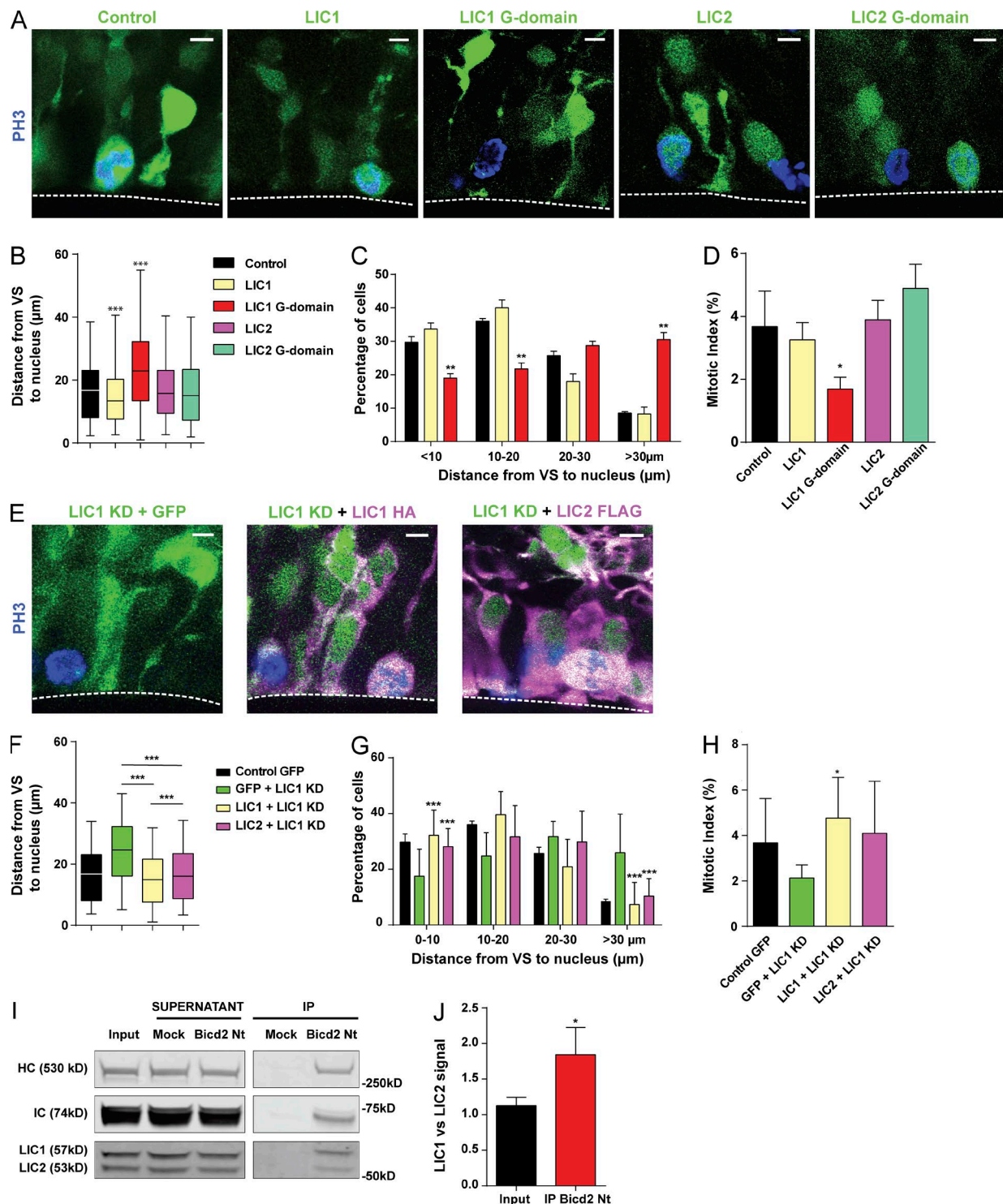
Figure 2. **Mechanisms contributing to the differential LIC roles in apical INM. (A–D)** E16 brains were in utero electroporated with control vector, the full-length, or G domain of either LIC. Analysis was performed at 4 d.p.i. **(A)** Fixed images of the VZ from electroporated brains stained for PH3. **(B and C)** Quantification of the distance between RGP nuclei and the VS across the various conditions. **(D)** Effect of the various cDNAs expression on RGP mitotic index. **(E–H)** shRNA for LIC1 was injected into the embryonic brain at E16 together with GFP alone, HA-tagged LIC1 RNAi-resistant, or FLAG-tagged standard LIC2 cDNA and analyzed 4 d.p.i. **(E)** Fixed images of the VZ from electroporated brains stained for PH3 and epitope tag. **(F and G)** Quantifications of the distance between RGP nuclei and the VS across the various conditions. **(H)** Mitotic index for the LIC1 rescue and LIC2 cross-rescue. Although statistically nonsignificant (P = 0.06), LIC2 partially reestablishes mitotic index. **(I and J)** BicD2 pull-down from embryonic rat brain lysate was evaluated for coimmunoprecipitation with dynein HC, IC, and LIC subunits. **(J)** Quantification of the signal intensity of LIC1 versus LIC2 in the input lane and the IP lane. Data presented as box-and-whiskers plot in B and F; data shown as mean ± SD in C, D, G, H, and J. Unpaired *t* test was used in B, C, D, F, G, H, and J. (*, P < 0.05; ***, P < 0.001). Data in B, C, and D include at least 343 RGPs from at least three embryos, and data in F, G, and H include at least 1,574 RGPs from at least six embryos. Data in J include four different pull-downs. Bars, 5 µm (A and E).

Gonçalves et al.
Dynein LIC1 and LIC2 in neocortical development

Journal of Cell Biology
https://doi.org/10.1083/jcb.201806112

811

Our results show that LIC1 is essential for BicD2-mediated apical INM. However, the ability of LIC2 to rescue RGP nuclear distribution and mitotic index in LIC1 KD cells suggests that the two LICs are each capable of binding to BicD2. To address this possibility, we incubated embryonic brain lysate with bacterially purified BicD2 N-terminal region, which binds dynein and its regulatory complex dynactin (Splinter et al., 2012; McKenney et al., 2014). Immunoblotting revealed that BicD2 bound both LICs, though LIC1 was significantly more enriched compared with LIC2 (Fig. 2, I and J). Therefore, although BicD2 can interact with either LIC, BicD2 preferentially recruits LIC1–dynein complexes. These results likely account for the predominant role of LIC1 in apical INM and the ability of overexpressed LIC2 to rescue apical INM when LIC1 is depleted.

LIC1 and LIC2 have distinct roles in post-mitotic neurons
We previously found that dynein is required for post-mitotic neuronal morphogenesis and subsequent migration into the CP, their final destination (Tsai et al., 2005, 2007). Therefore, we analyzed the distribution of electroporated cells in each of the neocortical layers upon depletion of the individual LICs. LIC1 KD caused a striking reduction in the number of neurons in the CP (Fig. 3, A and C), with most electroporated cells retained in the SVZ/IZ. In contrast, LIC2 KD had little effect in the progression of post-mitotic neurons to the CP (Fig. 3, A and C). Double LIC KD gave results similar to those effects for LIC1 KD alone (Fig. 3, A and C). Thus, we find that LIC1 is essential for both INM and neuronal migration to the CP, whereas LIC2 is dispensable for these cell behaviors.

Next, we tested the effects of expressing the full-length LICs and their G domains on neocortical cellular distribution. Expression of LIC1 or LIC2 full-length cDNA had no noticeable effect on the proportion of cells in the SVZ/IZ and CP (Fig. 3, B and D). Expression of the LIC2 G domain had no detectable effect on the proportion of cells in these regions either (Fig. 3, B and D), consistent with our LIC2 KD results. We note that there was a mild decrease in the number of cells in the VZ with LIC2 G domain expression, but the basis for this is unclear. In contrast to these conditions, expression of the LIC1 G domain caused severe accumulation of electroporated neurons in the SVZ/IZ and a marked reduction within the CP (Fig. 3, B and D), consistent with the effects of LIC1 KD.

As neurons migrate out of the IZ into the CP, they transition from a multipolar to bipolar migratory morphology. LIC1 KD caused a robust increase in the number of multipolar cells at the expense of bipolar cells (Fig. 3 E). In contrast, expression of the LIC1 G domain had no effect on the proportion of multipolar and bipolar neurons (Fig. 3 E), presumably reflecting a lesser degree of dynein inhibition. Once becoming bipolar in the SVZ/IZ, neurons initiate migration toward the CP using the glial (RGP) fibers as scaffolds, a mechanism known to require dynein (Tsai et al., 2007). Our results suggested that SVZ/IZ neurons expressing the LIC1 G domain were able to become bipolar, but were unable to migrate toward the CP. To test this hypothesis and determine whether LICs participate in glial-guided migration, we performed live imaging of the upper IZ/lower CP region and followed the migration of neurons transfected with control vector, LIC1 G domain, and LIC2 G domain. Neuronal cell bodies

expressing LIC1 G domain remained mostly immotile throughout the imaging period (Fig. 3 F and Videos 4 and 5). Expression of the LIC2 G domain had no significant effect, as cell bodies were able to migrate distances similar to those for control cells (Fig. 3 F and Video 6). Together, these results support fundamental roles for LIC1, but not LIC2, in the multipolar to bipolar transition and in glial-guided neuronal migration.

Novel role for dynein in terminal somal translocation of neurons
Despite the minimal role we found for LIC2 in INM, in the multipolar to bipolar transition and in glial-guided migration, LIC2 KD and LIC2 G domain expression caused a striking decrease in the number of cells reaching the uppermost layers of the CP (Fig. 4, A and B; and Fig. S3, A and B). The arrested cells also had elongated processes contacting the outer marginal zone (MZ), but their cell bodies were located in deeper neocortical layers compared with control (Fig. 4 C). This suggested an impairment of the last stage of neuronal migration, known as terminal somal translocation (TST). This behavior involves MZ contact and subsequent shortening of the leading process of the migrating neuron, as the soma continuously moves toward the pial surface of the brain (Nadarajah et al., 2001; Franco et al., 2011; Sekine et al., 2011). Unlike the preceding glial-guided neuronal migration along the RGP basal processes, TST does not use glial scaffolding, and the role of motor proteins is unexplored (Cooper, 2013).

To test LIC2 function in TST more directly, we performed live imaging of LIC2 G domain and LIC2 shRNA electroporated neurons in the upper CP. In control cells, the leading process contacted the MZ, and cell bodies migrated toward the pial surface as their leading process shortened (Fig. 4 D and Video 7). Processes of neurons expressing the LIC2 G domain or a LIC2 shRNA were elongated and still contacted the MZ, but the cell bodies remained immotile throughout the imaging period (Fig. 4 D, Video 8, Fig. S3 C, and Video 9), further confirming a key role for LIC2 in TST. To our knowledge, these results are the first to show a role for motor proteins in TST and identify a novel function for dynein during brain development.

LICs are required for neuronal migration in the post-natal rat brain
To determine the extent to which depleting LICs delays or permanently blocks neuronal migration, we introduced LIC1 or LIC2 shRNAs into E16 rat brain and analyzed neuronal distribution 2 wk later, at post-natal day 7 (P7; Fig. 5, A and B). LIC1 KD caused a marked accumulation of cell bodies in the white matter, with a reduction in the number of neurons in the post-natal neocortex, a striking outcome not observed in controls or in LIC2-depleted brains. In contrast, LIC2 KD neurons bypassed the white matter, though they were unable to migrate to the upper neocortical layers. These data are consistent with our results in the embryonic brain and further support our findings of fundamental, but distinct, roles for LIC1 and LIC2 in vivo.

Molecular roles of LICs in brain development
Notably, we find differences in LIC1 versus LIC2 phenotypes at multiple stages of neocortical development (Fig. 5 C). Expression
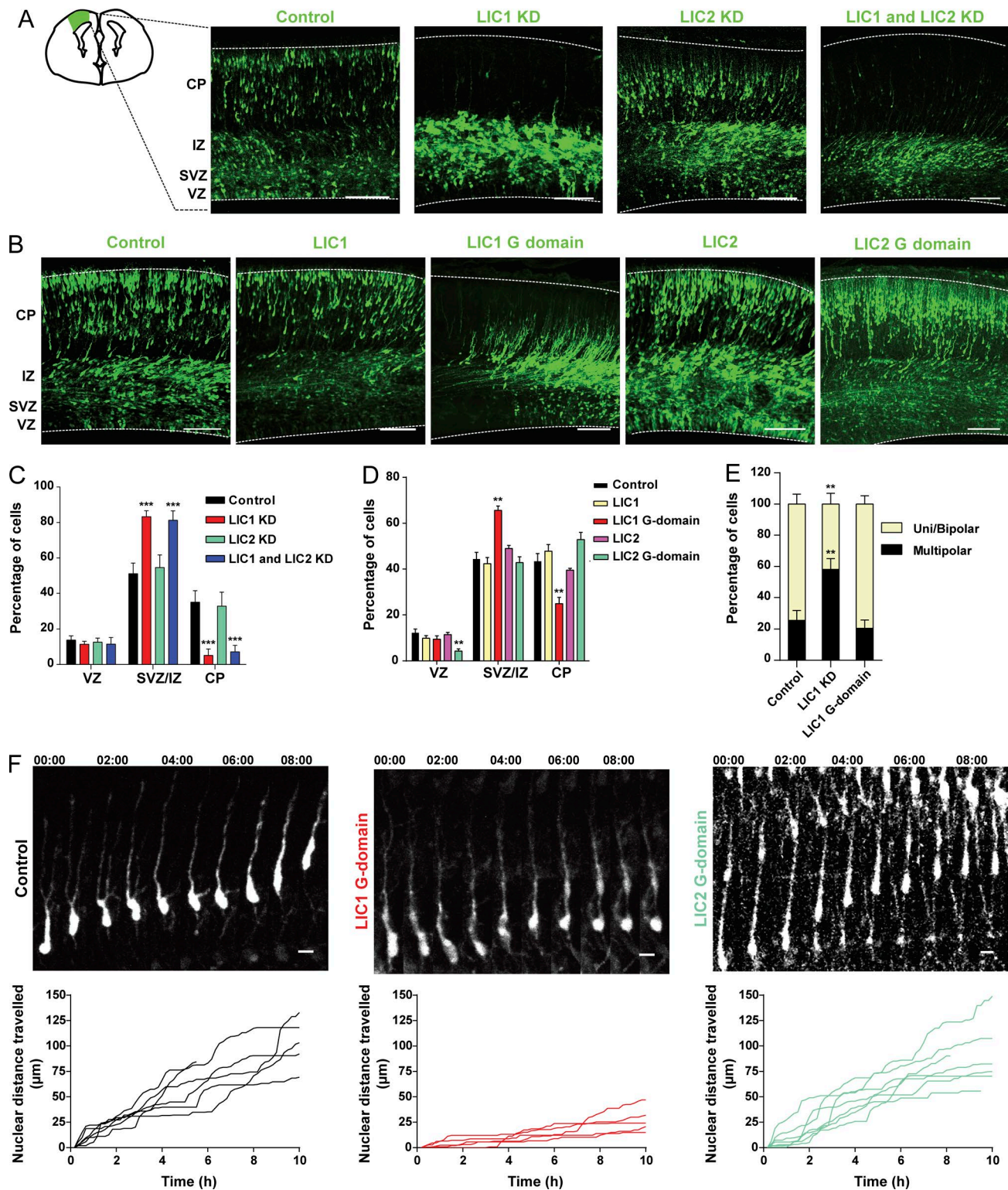
Figure 3. **Distinct roles for the LICs in post-mitotic neurons. (A–E)** E16 rat embryonic brains were in utero electroporated with shRNAs for LIC1 and/or LIC2, or functional domains of each LIC. Analysis was performed 4 d.p.i. **(A and B)** Images of the neocortex injected with control vector or shRNAs for LIC1 and/or LIC2 (A) and full-length or G domain versions of LIC1 or LIC2 (B). **(C and D)** Quantification of the proportion of transfected cells in each layer of the neocortex across conditions. **(E)** Quantification of the number of multipolar versus uni-/bipolar E20 neurons in the neocortex. **(F)** Time-lapse images for control, LIC1 G domain, or LIC2 G domain in migrating neurons (Videos 4, 5, and 6). Images are shown at 60-min intervals (hh:mm). Representative tracings are shown at the bottom. Data presented as mean ± SD. Unpaired t test was used in C, D, and E. (**, P < 0.01; ***, P < 0.001). Data in C include at least 2,130 cells from at least six embryos, data in D include at least 1,856 cells from at least three embryos, and data in E include at least 335 cells from at least five embryos. Bars: 100 μm (A and B); 10 μm (F).
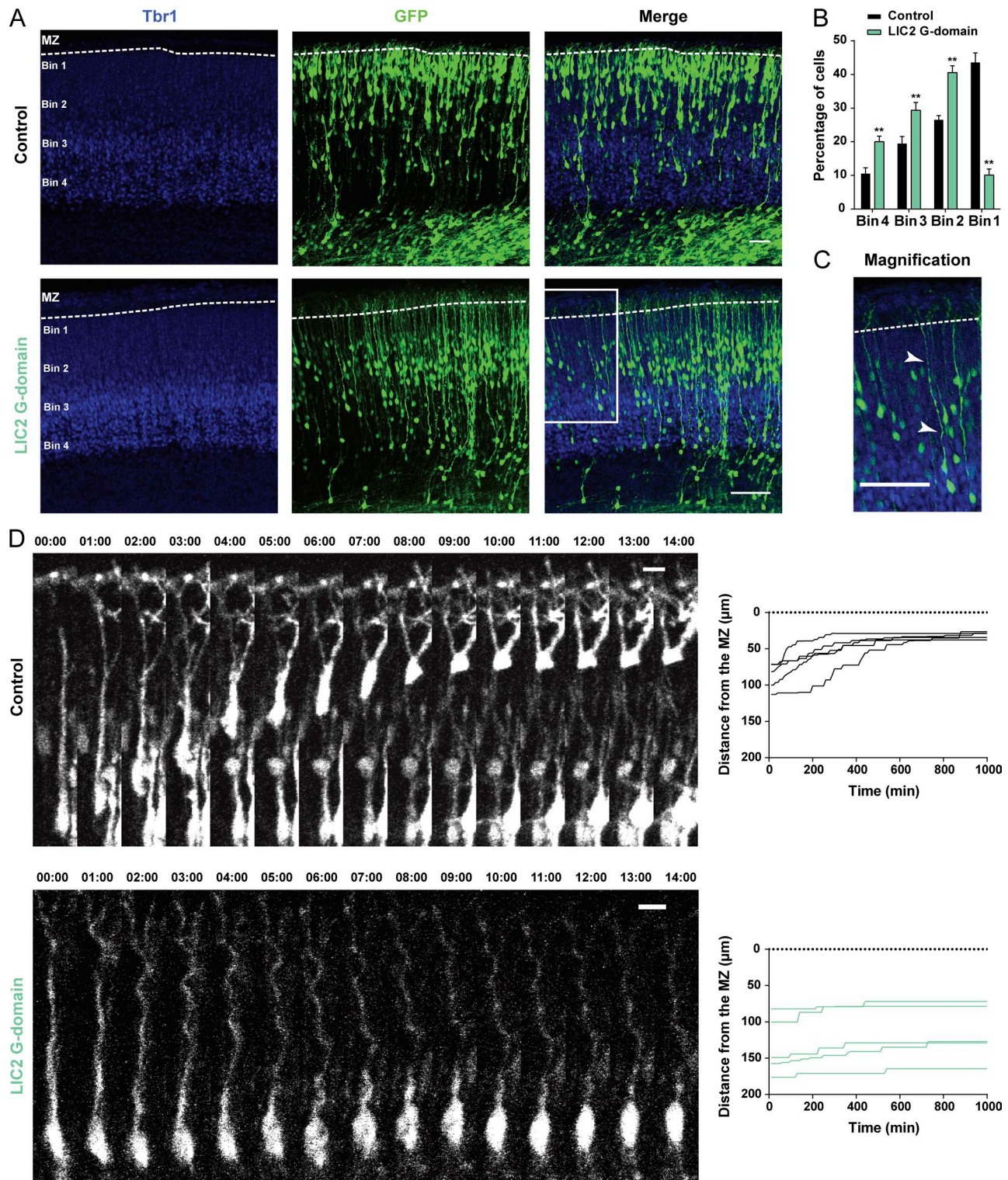
Figure 4.   **Dynein is required for TST of migrating neurons. (A–D)** E16 brains were in utero electroporated with control vector or LIC2 G domain and were analyzed by fixed and live imaging 4 d.p.i. Brain slices were stained for the post-mitotic neuronal marker, Tbr1. The CP was equally divided in bins for quantifications purposes. **(A)** Images of the CP for each condition. **(B)** Quantification of the proportion of electroporated cells in each bin of the CP. **(C)** Magnification of the delimited region in bottom right panel in A. Arrowheads mark the elongated migrating process. **(D)** Time-lapse images for control and LIC2 G domain in migrating neurons. Images are shown at 60-min intervals (hh:mm). Respective representative tracings from multiple migratory neurons for each condition are shown at right (Videos 7 and 8). Data are presented as mean ± SD in B, and unpaired *t* test was used (**, P < 0.01). Data in B includes at least 3,035 cells from at least six embryos. Bars: 40 µm (A and C); 10 µm (D).
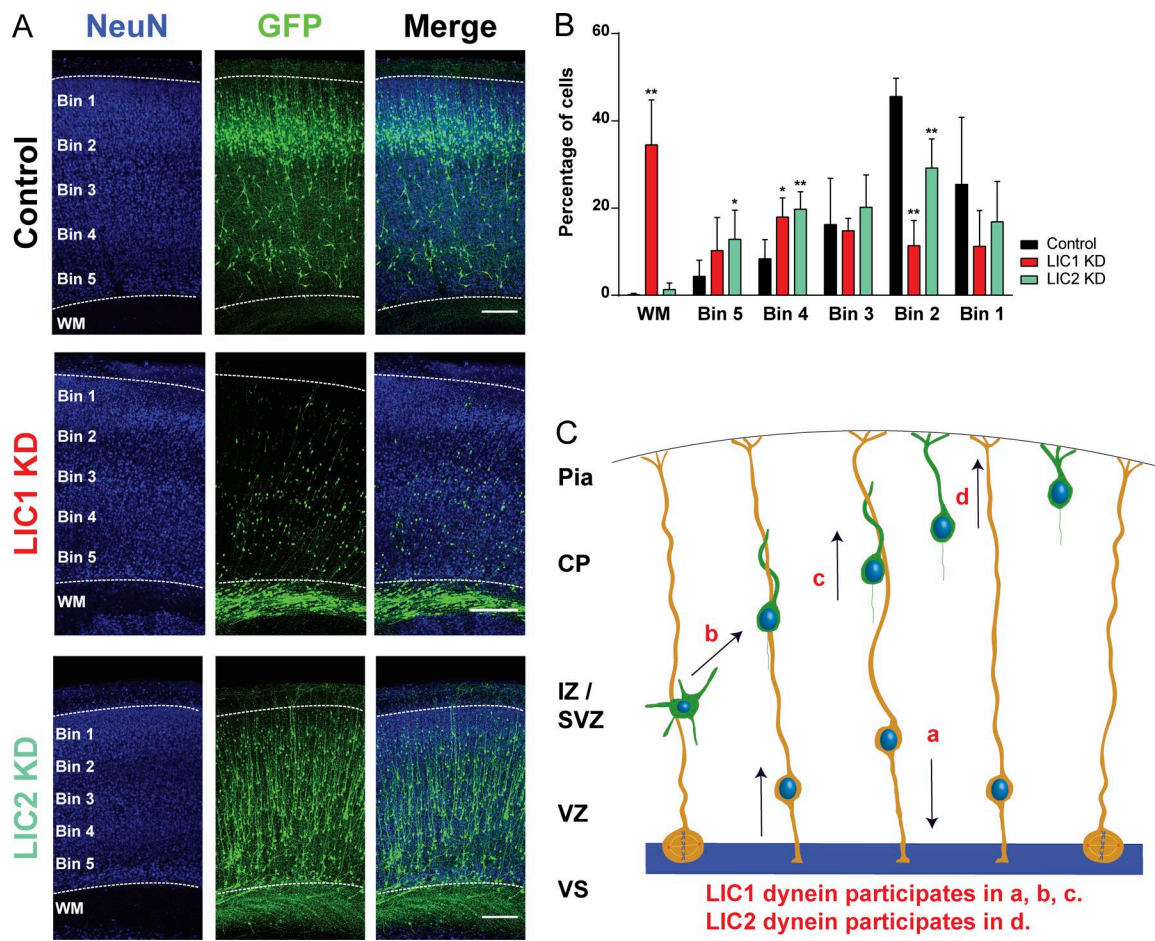
Figure 5. LIC inhibition severely impairs neuronal migration at post-natal stages. (A and B) E16 rat brains were in utero electroporated with control vector or shRNAs for LIC1 or LIC2. Analysis was done 2 wk after injection, at P7. Brain slices were stained for the mature neuronal marker, NeuN. The CP was equally divided in bins for quantifications purposes. **(A)** Images of the post-natal neocortex across conditions. Bar, 200 μm. **(B)** Quantification of the distribution of cells through the white matter and the CP. Data are presented as mean ± SD in B, and unpaired *t* test was used (*, P < 0.05; **, P < 0.01). Data in B include at least 1,215 cells from at least four pups, per condition. **(C)** Schematic illustration showing LIC roles in neocortical development. In yellow, RGPs undergoing INM. In green, multipolar post-mitotic neurons become bipolar and migrate to the CP. LIC1 participates in the apical nuclear migration of RGPs (a), the multipolar to bipolar transition (b), and glial-guided migration (c). LIC2 had no significant function in the previous behaviors, but plays an essential role in TST of neurons (d). WM, white matter.

of LIC1 shRNA or LIC1 G domain potently interfered with the dynein-driven apical INM. Similar analysis for LIC2 showed no detectable effect. Nonetheless, LIC2 overexpression completely rescued the LIC1 KD phenotype, indicating that abundant LIC2 is capable of serving in this function. Seeking to explain this surprising result, we found differences in LIC1 versus LIC2 binding to BicD2, the dynein adaptor in apical INM. We do note that other molecules interact differentially with the two LICs, most notably pericentrin and PAR3 (Purohit et al., 1999; Tynan et al., 2000a; Schmoranzer et al., 2009; Mahale et al., 2016). Conceivably, these interactions might also contribute, albeit subtly, to the phenotypic differences between the LICs that we observe.

Analysis of each LIC in post-mitotic neuronal migration revealed further differential roles. We found that LIC1 inhibition impedes newborn neurons from reaching the CP by disrupting at least two distinct mechanisms: the multipolar-to-bipolar transition and glial-guided migration. These results mimicked those for dynein HC KD (Tsai et al., 2005, 2007), which would disrupt overall dynein motor activity. LIC2 had no noticeable function

at these stages. Interestingly, BicD2 KD was reported to cause a multipolar accumulation at the expense of bipolar neurons (Hu et al., 2013), comparable to our results with LIC1 KD. This is consistent with a generally more substantial role for LIC1 in mediating BicD2-dependent functions, as seen in RGPs. Thus, we hypothesize that the BicD2–LIC1 interaction might be also active during multipolar to bipolar transition.

The minor role for LIC2 in earlier stages of brain development allowed us to uncover a novel role for dynein in neuronal TST. Neurons expressing LIC2 shRNA or LIC2 G domain reached the CP, but there was a marked accumulation of cell bodies abnormally far from the pial surface. We found that the processes of these cells were still able to contact the MZ, suggesting that LIC2 is not required for process extension, but is essential for somal translocation. Using live imaging, we confirmed this specific arrest in neuronal cell body movement. Although our results reveal a clear role for LIC2 in TST, we cannot determine whether LIC1 also has a role at this stage. This is because LIC1 inhibition severely impairs neuronal migration before this last step. We be-

lieve these results are the first evidence of a dynein role in TST. Thus, altogether, our data reveal a succession of dynein functions throughout neocortical development, which depends on differential roles of LICs at several stages.

The different LIC functions in brain development, primarily nonoverlapping, is consistent with earlier evidence that these dynein subunits exist in discrete LIC1- and LIC2-containing dynein subfractions as judged by coimmunoprecipitation studies (Tynan et al., 2000a). Our current study provides further insight into this issue and the mechanisms underlying differential LIC function. In particular, we find that expression of the LIC G domains strongly interferes with dynein function in vivo, as determined by the effects on neurogenesis and neuronal migration in the developing rat brain. A reasonable explanation for the inhibitory effect of the G domain expression would be the competition with endogenous LICs for the LIC binding site located within the tail region of the dynein HC. In this case, the prediction would be a similar phenotype from the expression of either LIC G domain. Surprisingly, however, the phenotypes are clearly distinct. For this reason, we speculate that each LIC might associate preferentially with dynein complexes of specific composition and/or post-translational modifications. Interestingly, a recent dynein interactome analysis detected an enrichment for different dynein light chain subunits in LIC1- versus LIC2-containing dynein (Redwine et al., 2017), suggesting to us that LIC integration into the dynein complex may depend on or dictate a specific dynein light chain subunit composition. How each LIC integrates the dynein complex likely contributes to the differential LIC1 and LIC2 functions in vivo, but the mechanisms for this remain to be determined.

Materials and methods

Ethics statement
All the experiments were done in accordance with the animal welfare guidelines and the guidance of the Institutional Animal Care and Use Committee at Columbia University (New York, NY).

In utero electroporation
Plasmids encoding for shRNAs or cDNA were injected into the developing brain at E16 and electroporated as described (Baffet et al., 2016). In more detail, timed pregnant Sprague Dawley E16 rats were anaesthetized with a ketamine xylazine cocktail administered intraperitoneally, and toe pinch was performed to ensure deep anesthesia. To avoid excessive heating loss during the surgical procedure, an external heating source was provided. For pain management, buprenorphine and bupivacaine were administered subcutaneously, before the surgery. Abdominal cavity was opened, and uterine horns were exposed and trans-illuminated for clear identification of the brain ventricles. For easy visualization of the DNA in the brain ventricular space, a nontoxic dye (Sigma, F7252) was added to the DNA before surgery and injected with a sharpened glass needle. After injection, embryos were subjected to five electric impulses (50 V; 50 ms each, separated by 1-s intervals) delivered by an electroporator (Harvard Apparatus ECM 830) to target the DNA to RGPs in the lateral neocortex. The embryos were returned to the abdominal cavity,

and the wound was closed. Rats were monitored every day after surgery, and buprenorphine was administered every 12 h for the first 48 h for post-operative pain control.

Immunohistochemistry and live imaging
For embryonic brain harvesting, pregnant rats were reanesthetized, and the surgical wound was reopened 4 d post injection (d.p.i.; at E20) to expose the uterus.

For fixed imaging, embryonic (E20) or P7 rat brains were harvested and immersed in PBS with 4% PFA overnight. They were then embedded in 4% of agarose (Sigma, A9539) and sliced in a vibratome (Leica, VT 1200S) in 100-μm slices for embryonic brains or 200-μm for P7 brains. After blocking in 5% normal donkey serum (Sigma, D9663) in PBS-Triton 0.5% for 1 h, slices were incubated with primary antibodies diluted in the blocking solution, overnight on a shaker, at 4°C. Secondary antibodies (1:500) and DAPI (Thermo Scientific, 62248; 1:10,000 dilution) were diluted in PBS and incubated for 2 h at room temperature. Slices were mounted with Aqua-Poly mounting media (Polysciences, 18606).

For live imaging, the dissected rat brains were embedded in 4% low-melting agarose (IBI Scientific, IB70057) diluted in artificial cerebrospinal fluid (Baffet et al., 2016) and sliced into 300-μm coronal sections. The slices were placed on porous filters (EMB Millipore, PICMORG50) in cortical culture medium containing 25% HBSS (Life Technologies, 24020-117), 47% basal MEM (Life Technologies, 21010-046), 25% normal horse serum (Life Technologies, 26050-088), 1% penicillin/streptomycin/glutamine (Life Technologies, 10378-016), and 2% of 30% glucose (Sigma, G5767) in a 50-mm glass-bottom dish (MatTek Corporation, P50G-0-14-F) and imaged on an IX80 laser scanning confocal microscope (Olympus FV1000 Spectral Confocal System) at intervals of 10 min for up to 24 h.

RNAi and constructs
shRNA expressing constructs were designed to target internal gene sequences unique to *Dync1li1* (LIC1) or *Dync1li2* (LIC2), in a pRetro-U6G vector (Cellogenetics), which also expressed soluble GFP to label-transfected cells. The target sequence for *Dync1li1* (LIC1) used was 5′-GTTGATTAGAGACTTCCAA-3′, and the target sequence for *Dync1li2* (LIC2) was 5′-GCCAGAAGATGCATATGAA-3′. Empty vector of pEGFP-C1 was used a control (Clontech). LIC1 and LIC2 rat cDNA constructs were taken from pCMV β (Tynan et al., 2000a) and cloned into pCAGIG vector (Addgene, plasmid no. 11159; Matsuda and Cepko, 2004) using NotI sites. Full-length and functional domain constructs of LIC1 and LIC2 were HA (YPY PVPDYA)- and FLAG (DYKDDDDK)-tagged, respectively (Tynan et al., 2000a). pCAGIG empty vector was used as control for the experiments with LIC1 and LIC2 full-length and functional domains. For better process visualization in the quantifications of Fig. 3 E and P7 experiments, shRNAs were coinjected with pCAG IG empty vector. Silent point mutations were made in LIC1 cDNA for RNAi resistance, and functional domains were amplified by PCR amplification using KOD Hot Start DNA Polymerase (Millipore, 71086). pIRES2 DsRed-Express2 BicD2 (Clontech) was described previously (Hu et al., 2013), and pDsRed-Express2-C1 (Clontech) was used as control. Soluble DsRed signal was en-

Gonçalves et al.
Dynein LIC1 and LIC2 in neocortical development

Journal of Cell Biology 816
https://doi.org/10.1083/jcb.201806112

hanced using anti-mCherry antibody (described below). BicD2 N-terminal 25–400 aa with an N-terminal strepII-SNAPf cassette (McKenney et al., 2014) was a gift from R. McKenney (University of California, Davis, Davis, California).

Western blot and coimmunoprecipitation
shRNAs and LIC functional domains were transfected in rat C6 brain glioma cells cultured in DMEM supplemented with 10% FBS and 1% penicillin/streptomycin and maintained at 37°C with 5% CO_2. Transfection of cultured cells with shRNAs for LIC1 or LIC2 and LIC1 and LIC2 G domains was performed using a Lonza Nucleofector kit V and an Amaxa Nucleofector, according to the manufacturer's instructions. Cells transfected with shRNAs and LIC functional domains were collected 72 h (for shRNAs) or 30 h (G domains) after transfection.

For brain samples, pregnant E16, E18, or E20 rats were anesthetized as described above. Embryonic brains were harvested, and the brains of the pregnant rats were used as the adult samples.

Cells transfected with shRNAs and brain samples were lysed on ice in Lysis Buffer (pH 7.2, 50 mM Tris-HCl, 150 mM NaCl, 1% Triton X-100, and 0.5% deoxycholic acid buffer) containing 1 mM DTT and a protease inhibitor cocktail (Sigma, P8340). Purified lysates were loaded on a polyacrylamide gel and transferred to a polyvinylidene difluoride membrane. The membrane was blocked in PBS with 0.5% powdered milk, incubated with primary antibodies diluted in PBS with 0.1% of powder milk, and washed and incubated with secondary LI-COR antibodies in PBS. Imaging of the blots was performed using an Odyssey system (LI-COR).

For the coimmunoprecipitation experiments in Fig. S2 (A and B), LIC G domain–transfected C6 cells were lysed with radioimmunoprecipitation assay buffer (pH 7.4, 50 mM Tris-HCl, 100 mM NaCl, 1 mM EGTA, and 0.5% NP-40) containing 1 mM DTT and a protease inhibitor cocktail on ice. Anti-HA (Abcam, ab137838) or anti-FLAG (Abcam, ab1162) antibodies were incubated with magnetic beads (Invitrogen, 10002D) for 1 h and then with cell lysates for 2 h. Blotting was performed as described above. For better separation of LIC1 (57 kD), LIC2 (53 kD), and antibody HC (50 kD) bands gel running was done for longer periods.

For the coimmunoprecipitation experiments in Fig. 2 (I and J), embryonic brains (E20) were lysed with brain buffer (pH 7.2, 50 mM Pipes, 50 mM Hepes, 2 mM $MgCl_2$, and 1 mM EDTA) containing DTT and a protease inhibitor cocktail and subjected to mechanical lysis in a dounce homogenizer on ice. SNAP-BicD2 was purified as described (McKenney et al., 2014) and incubated with Streptactin Sepharose beads (GE Life Sciences, 28-9355-99) for 1 h and then with brain lysates for 3 h. Blotting was performed has described above.

Antibodies
Antibodies used for immunofluorescence include anti-pH3 (Abcam, ab14955; 1:1,000), anti-Tbr1 (Abcam, ab31940; 1:300), anti-mCherry (Abcam, ab167453; 1:1,000), anti-NeuN (Millipore, MAB377; 1:300), anti-HA (Sigma-Aldrich, H6908; 1:2,000), anti-FLAG (Abcam, ab1162; 1:2,000), anti-LIC1 (Tan et al., 2011; 1:300), and anti-LIC2 (Tynan et al., 2000a; 1:300). Donkey fluorophore–conjugated secondary antibodies (Jackson Labs, 1:500 dilution) were used.

Antibodies used for Western blotting include anti-p150^{Glued} (BD, 610474; 1:1,000), anti–dynein IC clone 74.1 (University of Virginia, Charlottesville, VA; 1:1,000), anti-LICs (Tynan et al., 2000a; 1:500), anti-LIC1 (Tan et al., 2011; 1:500), anti-LIC2 (Tynan et al., 2000a; 1:1,000), anti–dynein HC (Suzuki et al., 2007; 1:1,000), and anti-GAPDH (Abcam, ab8245; 1:1,000). To develop in a LI-COR system, fluorescent secondary antibodies (1:10,000) were acquired from Invitrogen and Rockland.

Reverse transcription analysis
C6 cells were cultured and transfected with shRNAs for LIC1 and LIC2 using an Amaxa Nucleofector, as described for Western blot. mRNA extraction, cDNA synthesis, and quantitative PCR were performed using the Power SYBR Green Cells-to-Ct kit (Ambion/Thermofisher). cDNAs were analyzed by quantitative PCR using an ABI 7900 HT machine. Primers were designed to have melting temperatures of ~60°C degrees and to generate amplicons of 70–200 bp, separated by at least one intron. Target cDNA levels were analyzed by the comparative cycle method, and values were normalized to GAPDH expression levels. The primers used in this study were GAPDH forward: 5′-CAACTC CCTCAAGATTGTCAGCAA-3′; GAPDH reverse: 5′-GGCATGGAC TGTGGTCATGA-3′; *Dync1li1* (LIC1) forward: 5′-GGGAAAACA AGCCTCATAAGAAG-3′; *Dync1li1* (LIC1) reverse: 5′-AACTTGAGT AGCCCTTTGTGGTA-3′; *Dync1li2* (LIC2) forward: 5′-GACCCT GGTCATTTTTGTTGC-3′; and *Dync1li2* (LIC2) reverse: 5′-CCC GTAAAACACTAGCCCAT-3′.

Imaging and statistical analysis
All images were collected with an IX80 laser scanning confocal microscope (Olympus FV1000 Spectral Confocal System). Brain sections were imaged using a 60× 1.42 NA oil objective or a 10× 0.40 NA air objective. All images were analyzed using ImageJ software (National Institutes of Health).

All statistical analysis was performed using Prism (GraphPad Software). Unpaired t test (two-tailed) was used to determine significance between two groups. Statistical significance for LIC1 versus LIC2 signal (Fig. S1 D) was performed with one-way ANOVA followed by Tukey's test. Data distribution was assumed to be normal, but this was not formally tested. Definition of statistical significance was P < 0.05.

For each experiment, embryos were collected from at least three different mothers, for each condition. Mitotic index was measured as the percentage of electroporated RGP cells positive for PH3. The bars in the data presented as box and whiskers represent 1–99 percentile range.

Online supplemental material
Fig. S1 shows the RNAi KD efficiency and the LIC1 and LIC2 relative protein expression across brain development. Fig. S2 shows the effects of the G domains expression in the dynein complex and the effects of the A domains expression in RGP behavior. Fig. S3 shows the effects of LIC2 shRNA expression in neuronal TST. Videos 1, 2, and 3 show the effects of LIC inhibition in apical INM. Videos 4, 5, and 6 show the effect of LIC inhibition in glial-guided migration. Videos 7, 8, and 9 show the effects of LIC2 inhibition in neuronal TST.

Gonçalves et al.
Dynein LIC1 and LIC2 in neocortical development

Journal of Cell Biology
https://doi.org/10.1083/jcb.201806112

817

Acknowledgments

Author contributions: J.C. Gonçalves, T.J. Dantas, and R.B. Vallee conceptualized the work. J.C. Gonçalves did most of the experiments and data analysis. T.J. Dantas did the qRT-PCR experiments. R.B. Vallee was responsible for project administration and funding acquisition. T.J. Dantas and R.B. Vallee supervised the work. J.C. Gonçalves wrote the original manuscript draft. J.C. Gonçalves, T.J. Dantas, and Richard B. Vallee reviewed and edited the manuscript.

References

Baffet, A.D., D.J. Hu, and R.B. Vallee. 2015. Cdk1 Activates Pre-mitotic Nuclear Envelope Dynein Recruitment and Apical Nuclear Migration in Neural Stem Cells. *Dev. Cell.* 33:703–716. https://doi.org/10.1016/j.devcel.2015.04.022

Baffet, A.D., A. Carabalona, T.J. Dantas, D.D. Doobin, D.J. Hu, and R.B. Vallee. 2016. Cellular and subcellular imaging of motor protein-based behavior in embryonic rat brain. *Methods Cell Biol.* 131:349–363. https://doi.org/10.1016/bs.mcb.2015.06.013

Bertipaglia, C., J.C. Gonçalves, and R.B. Vallee. 2018. Nuclear migration in mammalian brain development. *Semin. Cell Dev. Biol.* 82:57–66. https://doi.org/10.1016/j.semcdb.2017.11.033

Carter, A.P., A.G. Diamant, and L. Urnavicius. 2016. How dynein and dynactin transport cargos: a structural perspective. *Curr. Opin. Struct. Biol.* 37:62–70. https://doi.org/10.1016/j.sbi.2015.12.003

Cooper, J.A. 2013. Mechanisms of cell migration in the nervous system. *J. Cell Biol.* 202:725–734. https://doi.org/10.1083/jcb.201305021

Doobin, D.J., S. Kemal, T.J. Dantas, and R.B. Vallee. 2016. Severe NDE1-mediated microcephaly results from neural progenitor cell cycle arrests at multiple specific stages. *Nat. Commun.* 7:12551. https://doi.org/10.1038/ncomms12551

Fiorillo, C., F. Moro, J. Yi, S. Weil, G. Brisca, G. Astrea, M. Severino, A. Romano, R. Battini, A. Rossi, et al. 2014. Novel dynein DYNC1H1 neck and motor domain mutations link distal spinal muscular atrophy and abnormal cortical development. *Hum. Mutat.* 35:298–302. https://doi.org/10.1002/humu.22491

Franco, S.J., I. Martinez-Garay, C. Gil-Sanz, S.R. Harkins-Perry, and U. Müller. 2011. Reelin regulates cadherin function via Dab1/Rap1 to control neuronal migration and lamination in the neocortex. *Neuron.* 69:482–497. https://doi.org/10.1016/j.neuron.2011.01.003

Gama, J.B., C. Pereira, P.A. Simões, R. Celestino, R.M. Reis, D.J. Barbosa, H.R. Pires, C. Carvalho, J. Amorim, A.X. Carvalho, et al. 2017. Molecular mechanism of dynein recruitment to kinetochores by the Rod-Zw10-Zwilch complex and Spindly. *J. Cell Biol.* 216:943–960. https://doi.org/10.1083/jcb.201610108

Grissom, P.M., E.A. Vaisberg, and J.R. McIntosh. 2002. Identification of a novel light intermediate chain (D2LIC) for mammalian cytoplasmic dynein 2. *Mol. Biol. Cell.* 13:817–829. https://doi.org/10.1091/mbc.01-08-0402

Hu, D.J.K., A.D. Baffet, T. Nayak, A. Akhmanova, V. Doye, and R.B. Vallee. 2013. Dynein recruitment to nuclear pores activates apical nuclear migration and mitotic entry in brain progenitor cells. *Cell.* 154:1300–1313. https://doi.org/10.1016/j.cell.2013.08.024

Jamuar, S.S., A.T. Lam, M. Kircher, A.M. D'Gama, J. Wang, B.J. Barry, X. Zhang, R.S. Hill, J.N. Partlow, A. Rozzo, et al. 2014. Somatic mutations in cerebral cortical malformations. *N. Engl. J. Med.* 371:733–743. https://doi.org/10.1056/NEJMoa1314432

Jones, L.A., C. Villemant, T. Starborg, A. Salter, G. Goddard, P. Ruane, P.G. Woodman, N. Papalopulu, S. Woolner, and V.J. Allan. 2014. Dynein light intermediate chains maintain spindle bipolarity by functioning in centriole cohesion. *J. Cell Biol.* 207:499–516. https://doi.org/10.1083/jcb.201408025

Kriegstein, A., and A. Alvarez-Buylla. 2009. The glial nature of embryonic and adult neural stem cells. *Annu. Rev. Neurosci.* 32:149–184. https://doi.org/10.1146/annurev.neuro.051508.135600

Lee, I.G., M.A. Olenick, M. Boczkowska, C. Franzini-Armstrong, E.L.F. Holzbaur, and R. Dominguez. 2018. A conserved interaction of the dynein light intermediate chain with dynein-dynactin effectors necessary for processivity. *Nat. Commun.* 9:986. https://doi.org/10.1038/s41467-018-03412-8

Lipka, J., M. Kuijpers, J. Jaworski, and C.C. Hoogenraad. 2013. Mutations in cytoplasmic dynein and its regulators cause malformations of cortical development and neurodegenerative diseases. *Biochem. Soc. Trans.* 41:1605–1612. https://doi.org/10.1042/BST20130188

Mahale, S., M. Kumar, A. Sharma, A. Babu, S. Ranjan, C. Sachidanandan, and S.V.S. Mylavarapu. 2016. The light intermediate chain 2 subpopulation of dynein regulates mitotic spindle orientation. *Sci. Rep.* 6:22. https://doi.org/10.1038/s41598-016-0030-3

Matsuda, T., and C.L. Cepko. 2004. Electroporation and RNA interference in the rodent retina in vivo and in vitro. *Proc. Natl. Acad. Sci. USA.* 101:16–22. https://doi.org/10.1073/pnas.2235688100

McKenney, R.J., W. Huynh, M.E. Tanenbaum, G. Bhabha, and R.D. Vale. 2014. Activation of cytoplasmic dynein motility by dynactin-cargo adapter complexes. *Science.* 345:337–341. https://doi.org/10.1126/science.1254198

Mikami, A., S.H. Tynan, T. Hama, K. Luby-Phelps, T. Saito, J.E. Crandall, J.C. Besharse, and R.B. Vallee. 2002. Molecular structure of cytoplasmic dynein 2 and its distribution in neuronal and ciliated cells. *J. Cell Sci.* 115:4801–4808. https://doi.org/10.1242/jcs.00168

Nadarajah, B., J.E. Brunstrom, J. Grutzendler, R.O. Wong, and A.L. Pearlman. 2001. Two modes of radial migration in early development of the cerebral cortex. *Nat. Neurosci.* 4:143–150. https://doi.org/10.1038/83967

Palmer, K.J., H. Hughes, and D.J. Stephens. 2009. Specificity of cytoplasmic dynein subunits in discrete membrane-trafficking steps. *Mol. Biol. Cell.* 20:2885–2899. https://doi.org/10.1091/mbc.e08-12-1160

Pfister, K.K., P.R. Shah, H. Hummerich, A. Russ, J. Cotton, A.A. Annuar, S.M. King, and E.M. Fisher. 2006. Genetic analysis of the cytoplasmic dynein subunit families. *PLoS Genet.* 2:e1. https://doi.org/10.1371/journal.pgen.0020001

Poirier, K., N. Lebrun, L. Broix, G. Tian, Y. Saillour, C. Boscheron, E. Parrini, S. Valence, B.S. Pierre, M. Oger, et al. 2013. Mutations in TUBG1, DYNC1H1, KIF5C and KIF2A cause malformations of cortical development and microcephaly. *Nat. Genet.* 45:639–647. https://doi.org/10.1038/ng.2613

Purohit, A., S.H. Tynan, R. Vallee, and S.J. Doxsey. 1999. Direct interaction of pericentrin with cytoplasmic dynein light intermediate chain contributes to mitotic spindle organization. *J. Cell Biol.* 147:481–492. https://doi.org/10.1083/jcb.147.3.481

Raaijmakers, J.A., M.E. Tanenbaum, and R.H. Medema. 2013. Systematic dissection of dynein regulators in mitosis. *J. Cell Biol.* 201:201–215. https://doi.org/10.1083/jcb.201208098

Reck-Peterson, S.L., W.B. Redwine, R.D. Vale, and A.P. Carter. 2018. The cytoplasmic dynein transport machinery and its many cargoes. *Nat. Rev. Mol. Cell Biol.* 19:382–398. https://doi.org/10.1038/s41580-018-0004-3

Redwine, W.B., M.E. DeSantis, I. Hollyer, Z.M. Htet, P.T. Tran, S.K. Swanson, L. Florens, M.P. Washburn, and S.L. Reck-Peterson. 2017. The human cytoplasmic dynein interactome reveals novel activators of motility. *eLife.* 6:1–27. https://doi.org/10.7554/eLife.28257

Reiner, O., R. Carrozzo, Y. Shen, M. Wehnert, F. Faustinella, W.B. Dobyns, C.T. Caskey, and D.H. Ledbetter. 1993. Isolation of a Miller-Dieker lissencephaly gene containing G protein beta-subunit-like repeats. *Nature.* 364:717–721. https://doi.org/10.1038/364717a0

Scherer, J., J. Yi, and R.B. Vallee. 2014. PKA-dependent dynein switching from lysosomes to adenovirus: a novel form of host-virus competition. *J. Cell Biol.* 205:163–177. https://doi.org/10.1083/jcb.201307116

Gonçalves et al.
Dynein LIC1 and LIC2 in neocortical development

Journal of Cell Biology 818
https://doi.org/10.1083/jcb.201806112

Schmoranzer, J., J.P. Fawcett, M. Segura, S. Tan, R.B. Vallee, T. Pawson, and G.G. Gundersen. 2009. Par3 and dynein associate to regulate local microtubule dynamics and centrosome orientation during migration. *Curr. Biol.* 19:1065–1074. https://doi.org/10.1016/j.cub.2009.05.065

Schroeder, C.M., and R.D. Vale. 2016. Assembly and activation of dynein-dynactin by the cargo adaptor protein Hook3. *J. Cell Biol.* 214:309–318. https://doi.org/10.1083/jcb.201604002

Schroeder, C.M., J.M. Ostrem, N.T. Hertz, and R.D. Vale. 2014. A Ras-like domain in the light intermediate chain bridges the dynein motor to a cargo-binding region. *eLife.* 3:e03351. https://doi.org/10.7554/eLife.03351

Sekine, K., T. Honda, T. Kawauchi, K. Kubo, and K. Nakajima. 2011. The outermost region of the developing cortical plate is crucial for both the switch of the radial migration mode and the Dab1-dependent "inside-out" lamination in the neocortex. *J. Neurosci.* 31:9426–9439. https://doi.org/10.1523/JNEUROSCI.0650-11.2011

Shu, T., R. Ayala, M.D. Nguyen, Z. Xie, J.G. Gleeson, and L.H. Tsai. 2004. Ndel1 operates in a common pathway with LIS1 and cytoplasmic dynein to regulate cortical neuronal positioning. *Neuron.* 44:263–277. https://doi.org/10.1016/j.neuron.2004.09.030

Splinter, D., D.S. Razafsky, M.A. Schlager, A. Serra-Marques, I. Grigoriev, J. Demmers, N. Keijzer, K. Jiang, I. Poser, A.A. Hyman, et al. 2012. BICD2, dynactin, and LIS1 cooperate in regulating dynein recruitment to cellular structures. *Mol. Biol. Cell.* 23:4226–4241. https://doi.org/10.1091/mbc.e12-03-0210

Suzuki, S.O., R.J. McKenney, S.Y. Mawatari, M. Mizuguchi, A. Mikami, T. Iwaki, J.E. Goldman, P. Canoll, and R.B. Vallee. 2007. Expression patterns of LIS1, dynein and their interaction partners dynactin, NudE, NudEL and NudC in human gliomas suggest roles in invasion and proliferation. *Acta Neuropathol.* 113:591–599. https://doi.org/10.1007/s00401-006-0180-7

Tan, S.C., J. Scherer, and R.B. Vallee. 2011. Recruitment of dynein to late endosomes and lysosomes through light intermediate chains. *Mol. Biol. Cell.* 22:467–477. https://doi.org/10.1091/mbc.e10-02-0129

Taylor, S.P., T.J. Dantas, I. Duran, S. Wu, R.S. Lachman, S.F. Nelson, D.H. Cohn, R.B. Vallee, and D. Krakow. University of Washington Center for Mendelian Genomics Consortium. 2015. Mutations in DYNC2LI1 disrupt cilia function and cause short rib polydactyly syndrome. *Nat. Commun.* 6:7092. https://doi.org/10.1038/ncomms8092

Tsai, J.W., Y. Chen, A.R. Kriegstein, and R.B. Vallee. 2005. LIS1 RNA interference blocks neural stem cell division, morphogenesis, and motility at multiple stages. *J. Cell Biol.* 170:935–945. https://doi.org/10.1083/jcb.200505166

Tsai, J.W., K.H. Bremner, and R.B. Vallee. 2007. Dual subcellular roles for LIS1 and dynein in radial neuronal migration in live brain tissue. *Nat. Neurosci.* 10:970–979. https://doi.org/10.1038/nn1934

Tsai, J.W., W.N. Lian, S. Kemal, A.R. Kriegstein, and R.B. Vallee. 2010. Kinesin 3 and cytoplasmic dynein mediate interkinetic nuclear migration in neural stem cells. *Nat. Neurosci.* 13:1463–1471. https://doi.org/10.1038/nn.2665

Tynan, S.H., M.A. Gee, and R.B. Vallee. 2000b. Distinct but overlapping sites within the cytoplasmic dynein heavy chain for dimerization and for intermediate chain and light intermediate chain binding. *J. Biol. Chem.* 275:32769–32774. https://doi.org/10.1074/jbc.M001537200

Tynan, S.H., A. Purohit, S.J. Doxsey, and R.B. Vallee. 2000a. Light intermediate chain 1 defines a functional subfraction of cytoplasmic dynein which binds to pericentrin. *J. Biol. Chem.* 275:32763–32768. https://doi.org/10.1074/jbc.M001536200